



# Boundary Condition for the Implementation of Arbitrary Acoustical Modes

Sina WITTHAUS<sup>1</sup>; Joerg R. SEUME<sup>2</sup>

Institute of Turbomachinery and Fluid Dynamics  
Leibniz Universität Hannover, Germany

## ABSTRACT

With the increase of bypass ratios of current jet engines, the dominating sound emission sources of aircraft engine noise consist of the tonal components of the fan and the compressor. Hence, the rotor-stator interaction noise is a significant contributor to the overall sound radiation from aircraft engines. The sound field consists of a superposition of various acoustical modes, generated by two effects: Firstly, the interaction of rotor wakes with the stator in each compressor stage and secondly, the relative rotation of potential fields of the cascades. Based on the blade and vane count and on the blade-passing frequency (BPF), the compressor modes that propagate can be estimated. Since the excited modes determine the emitted sound field, the numerical analysis of these acoustic structures is of great importance in understanding jet engine noise emissions. For this purpose, the sponge-layer boundary condition of the CAA-solver PIANO (developed by the German Aerospace Centre, DLR) is extended to implement arbitrary superposed modes. The FORTRAN-based code computes the resulting sound field in a cylindrical geometry, for a given set of azimuthal and radial mode orders, wavenumber and amplitudes of the modes to be excited. The numerically generated sound pressure distribution is validated against an analytical solution.

## NOMENCLATURE

### Latin Letters

|                |                                   |
|----------------|-----------------------------------|
| $a$            | speed of sound                    |
| $A, B$         | amplitudes of partial waves       |
| $C, D, E$      | proportionality factors           |
| $J_m$          | Bessel function of the first kind |
| $k$            | wavenumber                        |
| $L$            | length of sponge-layer            |
| $m$            | azimuthal mode order              |
| $Ma$           | Mach number                       |
| $n$            | radial mode order                 |
| $p'$           | acoustic pressure                 |
| $q$            | acoustic source term              |
| $R$            | outer duct radius                 |
| $r, \Theta, z$ | cylindrical coordinates           |
| $u', v', w'$   | sound particle velocities         |
| $U_0$          | uniform axial mean flow           |
| $u_{m,n}$      | eigenwert of the Bessel function  |

---

<sup>1</sup>witthaus@tfd.uni-hannover.de

<sup>2</sup>seume@tfd.uni-hannover.de

## Greek Letters

|                 |  |
|-----------------|--|
| $\alpha_{m,n}$  | modal axial wavenumber                       |
| $\beta_{m,n}$   | modal radial wavenumber                      |
| $\gamma$        | exponent of fading function                  |
| $\lambda_{ax}$  | axial wavelength                             |
| $\omega$        | angular frequency                            |
| $\phi$          | mode propagation angle in $z - \Theta$ plane |
| $\rho$          | density                                      |
| $\rho'$         | acoustic density                             |
| $\varphi$       | state quantity                               |
| $\xi_{cut-off}$ | cut-off ratio                                |

## 1. INTRODUCTION

The main contributors to the overall sound emission from aircraft engines have been displaced in the last few years. Due to an increase of bypass ratio of modern turbojet engines, the jet velocity has diminished (1). As a result, jet noise decreases as it is a function of jet exit velocity. Hence, noise components of the fan and the core engine are now the main focus of attention in noise reduction. The tonal components of fan and core engine noise are mainly produced by rotor-stator interaction. The generation of sound due to the relative motion of rotors and stators to each other is based on two mechanisms (2). One effect can be described as an interaction of wakes from blades, vanes or struts with the adjacent downstream vanes or blades. This causes unsteady forces on the airfoils, which then induce sound sources on the blade/vane surface. The second mechanism, the potential interaction, imposes unsteady forces due to the relative rotation of the lift distribution of the blades/vanes with a finite thickness on the adjacent vane/blade rows. The described generation of sound sources by rotor-stator interaction leads to rotating pressure patterns, so called spinning modes (3, 4). These acoustical modes dominate the tonal sound emission from rotating turbomachinery. The first extensive analysis of modes, generated by rotating cascades, is reported by Tyler and Sofrin (4). In their work they derive a correlation between the number of vanes and blades, the shaft speed, and the generated azimuthal modes. The propagation or decay of a mode depends on the excitation frequency, geometric dimensions, and thermodynamic state.

In the last few years, several computational approaches have been developed to address the problem of acoustic mode generation and propagation through turbomachinery. Özyörük and Long (5) used a time-dependent Euler-Code for near-field computations in combination with the method of Kirchhoff (6) for far-field predictions. Schnell (7) used a time-domain RANS approach to solve tonal noise of a fan stage, allowing arbitrary blade counts. A hybrid approach, using CFD (Computational Fluid Dynamics) and CAA (Computational AeroAcoustics) techniques, is presented by Weckmüller et al. (8). For the unsteady source region the CFD-solver TRACE (DLR<sup>1</sup>) was used to calculate the aerodynamic flow field and the sound sources. The flow solution was coupled to the sound field calculations in the CAA-solver PIANO (DLR) via interpolation through an interface.

Hybrid CFD/CAA approaches have proven to be more efficient in terms of computational cost compared to pure CFD methods. CFD methods require a spatial discretization resolution of 40 to 50 points per wavelength (PPW) (8, 9), whereas for low-dissipative CAA methods (cf. Tam and Webb (10)) a resolution of 7 PPW is sufficient. In the present work, an indirect coupling method for CFD/CAA simulations is presented. The existing sponge-layer boundary condition in PIANO (11) is extended to implement arbitrary acoustic modes in circular duct geometries. Since in turbomachinery applications multiple modes are generated and propagate through the ducts and channels, the developed boundary condition allows a superposition of selected dominant modes. Thus, in future investigations the modal noise components, calculated with unsteady CFD, can easily be implemented into CAA calculations, aimed at mode propagation analyses in e.g. inlet/outlet ducts, pipes and flow channels.

## 2. THE CAA-SOLVER PIANO

The CAA code PIANO (Perturbation Investigation of Aerodynamic Noise) was developed by the Institute of Aerodynamics and Flow Technology of the German Aerospace Center (DLR) (11). PIANO is a FORTRAN-

<sup>1</sup>German Aerospace Center

based code intended for three-dimensional, acoustic time domain simulations based on RANS calculations of a non-uniform background flow. The spatial discretization is accomplished with Tam and Webb's dispersion-relation-finite difference scheme of 4th order (11, 10). This optimized discretization in wavenumber space, ensures an accurate propagation of the sound waves (10, 12). To minimize the dissipation and dispersion errors of the time discretization, the low-dissipation and low-dispersion Runge-Kutta (LDDRK) scheme, presented by Hu et al. (13), is used (11). In PIANO, two sets of equations are available: the linearized Euler equations (LEE) or the acoustic perturbation equations (APE). For the current work the LEE are used.

## 2.1 Sponge-Layer

PIANO applies different kinds of sponge-layer types. A sponge-layer boundary condition is defined along multiple nodes of the CAA mesh to either implement acoustic sources or to provide acoustic damping, in order to avoid reflections at domain boundaries. In general, the sponge-layer boundary enforces defined forcing functions on the source term  $q$  of the LEE (11, 14):

$$q = -\sigma(x) (\varphi_{\text{computed}} - \varphi_{\text{forcing function}}), \quad (1)$$

with an arbitrary quantity  $\varphi$  (here: pressure, density, sound particle velocities). A fading function  $\sigma(x)$ , dependent on the distance from the wall, is employed to launch the defined forcing function gradually (14)

$$\sigma(x) = \sigma_{\max} \left| 1 - \frac{x-L}{L} \right|^\gamma. \quad (2)$$

$L$  denotes the length of the sponge-layer and  $\gamma$  the exponent of the fading function. The magnitude  $\sigma_{\max}$  is usually set to  $\sigma_{\max} > 100$  to ensure the initialization of the forcing function. Consequently, the solution at  $x = 0$  corresponds to the forcing functions, whereas for  $x = L$  the solution of the LEE applies. This approach prevents reflections at the boundary between the sponge-layer and the acoustic domain. Depending on the particular application, the depth of the sponge-layer, and the magnitude of the fading function can be adjusted.

To implement arbitrary acoustic modes via a sponge-layer boundary condition, the forcing functions, defining the variables  $\varphi_{\text{forcing function}}$ , need to be manipulated such that the chosen modes are imposed upon the acoustic domain. The governing equations of mode propagation in cylindrical coordinates are derived in the following chapter.

## 3. FORCING EQUATIONS FOR DUCT MODES

For a circular duct with a uniform mean flow the acoustic wave equation in cylindrical coordinates  $r, \Theta, z$  is given by

$$\frac{1}{a^2} \frac{D^2 p'}{Dt^2} - \frac{1}{r} \frac{\partial}{\partial r} \left( r \frac{\partial p'}{\partial r} \right) - \frac{1}{r^2} \frac{\partial^2 p'}{\partial \Theta^2} - \frac{\partial^2 p'}{\partial z^2} = 0, \quad (3)$$

with the speed of sound  $a$  and the acoustic pressure perturbation  $p'$ . Using the condition of acoustically hard walls and mode propagation in the positive axial direction, the solution of Eq. (3) for one pair of modes  $m, n$  yields

$$p'_{m,n}(z, r, \Theta, t) = \underbrace{(A_3 e^{-im\Theta} + B_3 e^{im\Theta})}_{\text{azimuthal}} \cdot \underbrace{A_2 J_m(\beta_{m,n} r)}_{\text{radial}} \cdot \underbrace{A_1 e^{-i\alpha_{m,n}^+ z}}_{\text{axial}} \cdot e^{i\omega t}, \quad (4)$$

where  $A_{1,2,3}$  and  $B_{1,3}$  denote the complex amplitudes of the partial waves in azimuthal, radial, and axial direction, respectively. The Bessel function of the first kind  $J_m$  determines the pressure distribution in radial direction subject to the radial wavenumber  $\beta_{m,n} = \frac{u_{m,n}}{R}$ . Taking into account a homogeneous and homentropic axial mean flow with Mach number  $Ma$  the axial wavenumber is given by

$$\alpha_{m,n}^+ = \frac{-kMa + \sqrt{k^2 - (1 - Ma^2)\beta_{m,n}^2}}{(1 - Ma^2)}. \quad (5)$$

The assumption of a steady and uniform mean flow is sufficient, since the main applications for the sponge-layer approach are duct inlets and exits, outside the unsteady flow regions. Here, axial flow discrepancies and rotational velocities can be neglected. An acoustical mode only propagates in axial direction if  $\alpha_{m,n}$  is real. Since the sound field in a duct is always a superposition of all modes that propagate, the overall sound field is described with

$$p'(z, r, \Theta, t) = \sum_{m=0}^{\infty} \sum_{n=0}^{\infty} p'_{m,n}(z, r, \Theta, t). \quad (6)$$

For the implementation of the acoustic modes, altogether 5 forcing equations for the acoustic perturbation quantities are needed: for the pressure  $p'_{m,n}$  (cf. Eq. (4)), the density  $\rho'$ , and the sound particle velocities  $u', v', w'$ . The distribution of the acoustic density corresponds to the pressure's of Eq. (4)

$$\rho'_{m,n} = p'_{m,n}. \quad (7)$$

The sound particle velocities are derived under the assumption of a proportional coherence to the sound pressure  $p'_{m,n}$ :

$$u'_{m,n} = C \cdot p'_{m,n} \quad (8)$$

$$v'_{m,n} = D \cdot p'_{m,n} \quad (9)$$

$$w'_{m,n} = E \cdot p'_{m,n} \quad (10)$$

Since  $p'_{m,n}$  is given by Eq. (4), the missing factors  $C, D, E$  are obtained using the Euler equations for inviscid flows without volume forces

$$\rho \frac{Du_i}{Dt} = -\frac{\partial p'}{\partial x_i}. \quad (11)$$

For a uniform mean flow  $U_0$  in axial direction  $z$  Eq. (11) yields

$$\frac{\partial u'}{\partial t} + U_0 \frac{\partial u'}{\partial z} = -\frac{1}{\rho} \frac{\partial p'}{\partial z}. \quad (12)$$

Deriving the temporal and spatial derivatives of  $u'$  from Eq. (12) with Eq. (8), the proportionality factor  $C$  for  $u'$  is derived as

$$C = \frac{1}{\rho} \frac{\alpha_{m,n}}{\omega - U_0 \alpha_{m,n}^+}. \quad (13)$$

The same approach is thus used to obtain the factors for the circumferential direction

$$\frac{\partial w'}{\partial t} + U_0 \frac{\partial w'}{\partial z} = -\frac{1}{\rho r} \frac{\partial p'}{\partial \Theta} \quad (14)$$

$$D = -\frac{m}{\rho r \cdot (\omega - U_0 \alpha_{m,n}^+)} \cdot \frac{B_3 e^{im\Theta} - A_3 e^{-im\Theta}}{B_3 e^{im\Theta} + A_3 e^{-im\Theta}} \quad (15)$$

and the radial direction

$$\frac{\partial v'}{\partial t} + U_0 \frac{\partial v'}{\partial z} = -\frac{1}{\rho} \frac{\partial p'}{\partial r} \quad (16)$$

$$E = -\frac{\beta_{m,n}}{2\rho} \frac{J_{m-1}(u_{m,n}) - J_{m+1}(u_{m,n})}{iJ_m(\beta_{m,n}r) \cdot (\omega - U_0 \alpha_{m,n}^+)}. \quad (17)$$

Based on Eq. (4) and Eq. (8)-(10) the sound field of a single mode can be described. For superposed modes, the sum of all forcing equations (cf. Eq. (6)) constitute the overall sound field. The named equations serve as the forcing functions  $\varphi_{\text{forcing function}}$  described in Sec. 2.1.

### 3.1 Implementation Strategy

In order to initialize specific sound sources in the acoustical domain in PIANO, a specific input file is read during the initialization of PIANO. Here, the input file is modified such that selected modes are induced by the forcing functions of Sec. 3. For this, variables have to be determined that define the modal structure of pressure, density, and sound particle velocities distinctly. Thus, the user-defined variables are

- Azimuthal mode order  $m$
- Radial mode order  $n$
- Wavenumber  $k$
- Amplitude in positive azimuthal direction  $A_3$
- Amplitude in negative azimuthal direction  $B_3$
- Amplitudes of radial an axial parts  $A_{1,2}$
- Duct radius  $R$

The above-named quantities are stored in a FORTRAN structure which enlarges in dimension, dependent on the mode count that is defined by the user. For every induced mode, the state variables are computed according to Eq. (4), (8)-(10) for every time step in the simulation. The overall sound field is obtained by adding the partial solutions corresponding to Eq. (6). The generated sound field is imposed upon the acoustic domain according to Eq. (1).

#### 4. CODE VALIDATION

To assess the reliability of the numerical approach for mode implementation, various mode combinations are computed. For that purpose, a uniform duct geometry with radius  $R$  and length  $10R$  is used (cf. Fig. 1). The sponge-layer is oriented into the positive axial direction, since the forcing equations only account for mode propagation in the positive axial direction. The duct walls are defined as acoustically hard walls. At the duct exit, a damping sponge-layer is applied to avoid reflections that might affect source implementation at the inlet. In case of a background flow, the flow direction is opposite to the mode propagation, as is characteristic for turbomachinery inlet ducts. The numerical results are compared with analytical solutions for the azimuthal

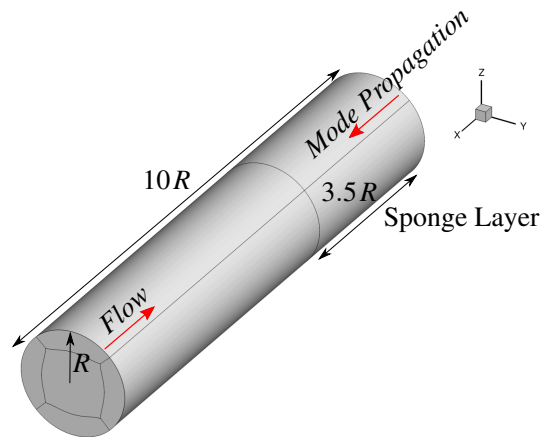


Figure 1 – Numerical setup for CAA simulations in PIANO: duct geometry with sponge-layer boundary condition.

and radial pressure distributions in a circular duct.

In the present work, the focus is on mode implementation, hence the mode propagation is not examined. Therefore, the sound pressure samples are exported close to the origin of the sponge-layer. First, the accuracy of implementing defined mode orders is examined using the example of standing modes, complemented by an investigation of the mean flow dependence. Subsequent, the capability of implementing spinning and superposed modes is studied.

In a first analysis, defined modes are excited separately. The amplitudes  $A_{1,2,3}$  and  $B_3$  are chosen in a way such that standing modes are generated. To ensure mode generation, the wavenumber  $k$  is selected so that a cut-off ratio  $\xi_{cut-off} = \frac{k}{k_{cut-off}} \geq 1$  applies (cf. Tab. 2). The pressure distribution of the calculated test cases

Table 2 – Generation of standing acoustical modes

| $m, n$ | $A_{1,2}$ | $A_3$ | $B_3$ | $\xi_{cut-off}$ |
|--------|-----------|-------|-------|-----------------|
| 1,2    | 1         | 1     | 1     | 1.01            |
| 2,0    | 1         | 1     | 1     | 1.02            |
| 2,1    | 1         | 1     | 1     | 1.01            |
| 3,0    | 1         | 1     | 1     | 1.02            |
| 3,3    | 1         | 1     | 1     | 1.00            |
| 7,0    | 1         | 1     | 1     | 1.00            |

is shown in Fig. 2. All executed simulations show robust and stable behavior. To verify the validity of the implemented mode structures, the azimuthal and radial pressure distributions are compared to the analytical solution. Exemplarily, the azimuthal pressure patterns of the modes  $m, n = (2, 1), (3, 3), (7, 0)$  at the duct wall are shown on the left hand side of Fig. 3. The numerical results in the sponge-layer fit well to the analytical values. The percentage deviations from the analytical solution for all computations of Tab. 2 are below 1%, with the highest aberration of 0.7% for mode  $m, n = (7, 0)$ . Furthermore, the radial pressure patterns from the CAA simulations in PIANO are in good accordance with analytic solutions, as well (right hand side Fig. 3). Here, the maximum deviation of 1,2% is found for  $m, n = (1, 2)$  (not shown). It should be noted that the observed aberrations are differences in amplitude, not in phase. The numerical results show a sufficient accuracy for standing modes in relation to the analytical solution of the wave equation.

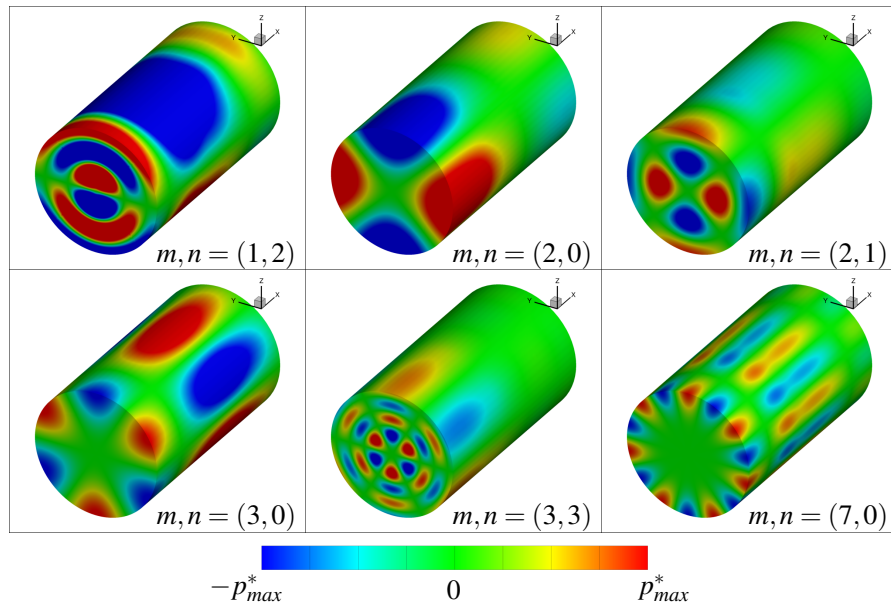


Figure 2 – Contour plots of the sponge-layer - dimensionless sound pressure  $p^*$ .

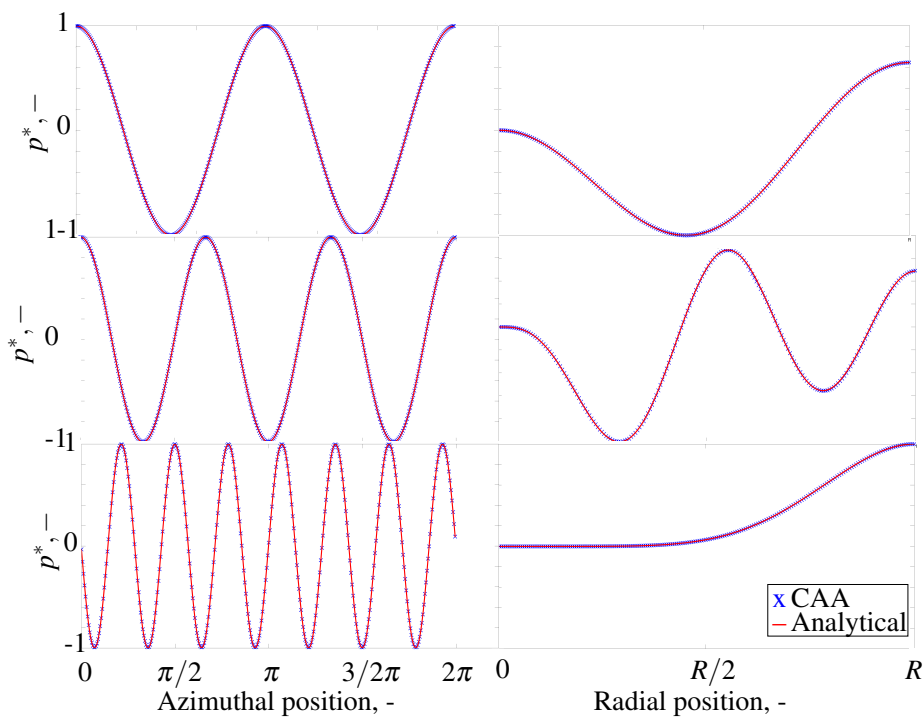


Figure 3 – Dimensionless pressure distributions for  $m, n = (2, 1), (3, 3), (7, 0)$  (top down).

The newly developed boundary condition takes into account a uniform mean flow in axial direction. It is assumed that radial fluctuations and swirl can be neglected at a sufficient distance from the rotating turbomachinery components. The axial mean flow affects the axial wavenumber  $\alpha_{m,n}$  and therefore the mode's cut-on frequency and axial wavelength. It is expected that with increasing Mach number and for upstream propagating modes, the axial wavelength contracts. The axial wavelengths of the standing mode  $m,n = (2,0)$ , propagating at different mean flows are examined:

|                 |                 |                          |                 |             |           |
|-----------------|-----------------|--------------------------|-----------------|-------------|-----------|
| 1. $Ma = 0$ :   | $m,n = (2,0)$ , | $\xi_{cut-off} = 2.58$ , | $A_{1,2} = 1$ , | $A_3 = 1$ , | $B_3 = 1$ |
| 2. $Ma = 0.2$ : | $m,n = (2,0)$ , | $\xi_{cut-off} = 2.58$ , | $A_{1,2} = 1$ , | $A_3 = 1$ , | $B_3 = 1$ |
| 3. $Ma = 0.4$ : | $m,n = (2,0)$ , | $\xi_{cut-off} = 2.58$ , | $A_{1,2} = 1$ , | $A_3 = 1$ , | $B_3 = 1$ |

The axial wavelength is given by

$$\lambda_{ax} = \frac{2\pi}{\alpha_{m,n}} \quad (18)$$

and therefore the analytical values for the three test cases are  $\lambda_{ax, Ma=0} = 0.085 m$ ,  $\lambda_{ax, Ma=0.2} = 0.069 m$ , and  $\lambda_{ax, Ma=0.4} = 0.049 m$ . To obtain the axial wavelengths from the PIANO computations, pressure distributions along the duct axis at the duct walls are exported. A subsequent spatial Fourier analysis yields the spatial frequency and therewith  $\lambda_{ax}$ . The results from PIANO are presented in Fig. 4. The dominant frequencies give the axial wavelengths for the different test cases:

- $\lambda_{ax, Ma=0} = 0.083 m$
- $\lambda_{ax, Ma=0.2} = 0.067 m$
- $\lambda_{ax, Ma=0.4} = 0.050 m$

The results are in good agreement with the analytical solutions.

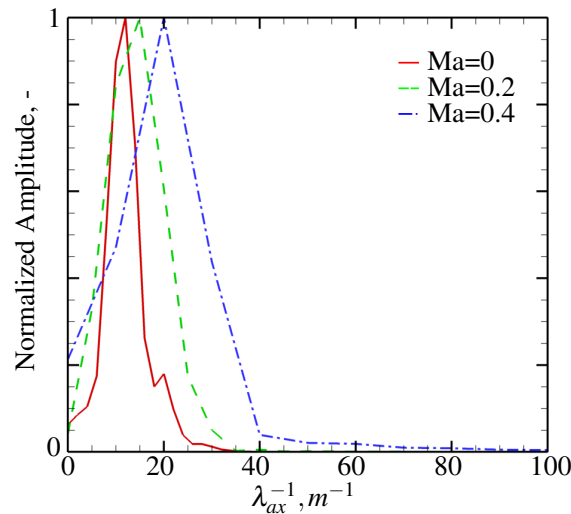


Figure 4 – Spatial frequency of axial pressure distributions for  $m,n = (2,0)$  at different Mach numbers.

Whether the generated modes are standing or spinning modes depends on the proportion of the partial wave amplitudes of Eq. (4) to each other. In general, the acoustic pressure patterns of turbomachinery inlets or outlet channels are dominated by spinning modes, which is why the developed boundary condition of this work must incorporate an accurate implementation of modes with rotational speed. As shown by Rice et al. (?), the wave propagating angle in the  $z - \Theta$  plane, relative to the duct axis, is defined as

$$\phi = \arctan\left(\frac{m}{\alpha_{m,n} \cdot r}\right). \quad (19)$$

If a spinning mode of order  $m,n = (3,0)$ , propagating at a wavenumber  $k = 43$  with amplitudes  $A_3 = 1$ ,  $B_3 = 0$  is considered, Eq. (19) yields  $\phi = 73^\circ$  for the test case considered. By analogy, for  $m,n = (1,0)$ ,  $k = 19$  and  $A_3 = 1$ ,  $B_3 = 0$  the propagation angle is  $\phi = 65^\circ$ . Taking the wavefronts from the CAA simulation at a position within the sponge-layer, the calculated angles agree well with the computed sound field (cf. Fig. 5). The azimuthal and radial pressure patterns as well show a maximum deviation less than 1% compared to the analytical solution.

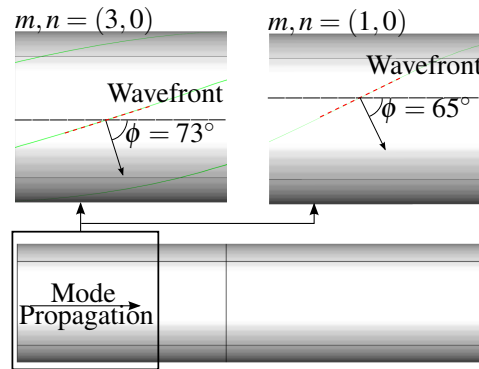


Figure 5 – Mode propagation angles of spinning modes  $m, n = (3, 0)$  and  $m, n = (1, 0)$  .

The sound field in ducts, pipes, and all enclosed channels is always a superposition of all cut-on modes. Hence, the implementation of a realistic sound field emitted from turbomachinery requires the capability to superpose modes. To test the accuracy of the code with regard to the superposition of modes, a test case with two counterrotating modes with the same mode order is simulated:

1.  $\theta^+$ -rotating mode:  $m, n = (1, 0)$ ,  $\xi_{cut-off} = 2.11, A_{1,2} = 1, A_3 = 1, B_3 = 0$
2.  $\theta^-$ -rotating mode:  $m, n = (1, 0)$ ,  $\xi_{cut-off} = 2.11, A_{1,2} = 1, A_3 = 0, B_3 = 1$

Given that the above-named modes propagate with the same order of amplitudes, the superposition of the modes results in a standing mode  $m, n = (1, 0)$ . Again, the pressure distributions fit the analytical solution quite well. The deviation is less than 0.1%. The analytical axial wavelength  $\lambda_{ax}$  for the standing mode is  $\lambda_{ax} = 0.177 m$ . The result of a spatial Fourier analysis of an axial pressure distribution in the sponge-layer is shown in Fig. 6. The resulting axial wavelength of the CAA simulation is consequently  $\lambda_{ax} = 0.175 m$ , which

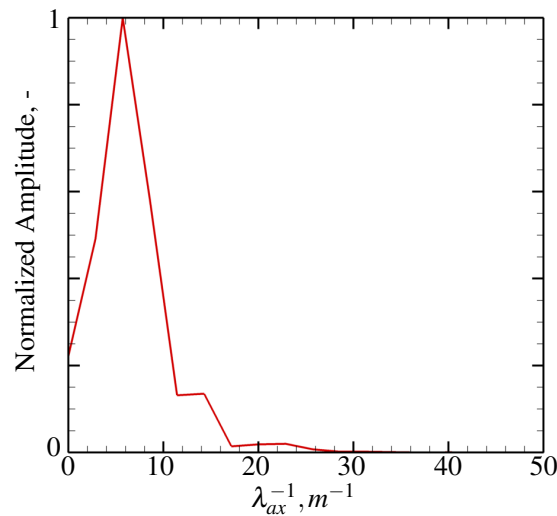


Figure 6 – Spatial Fourier analysis of an axial pressure distribution along the sponge-layer.

corresponds to an aberration of 1.1%. The test case proves that the presented sponge-layer boundary condition allows the implementation of superposed modes with high accuracy.

## 5. CONCLUSIONS

An extension of the sponge-layer boundary condition of the code PIANO is presented and validated. The extension aims at the sound generation of rotating turbomachinery due to rotor-stator interaction. For that purpose, the forcing functions of the sponge-layer boundary condition are manipulated such that arbitrary modes can be implemented accounting for a uniform mean flow. The resulting sound field is a superposition of all cut-on modes. The presented boundary condition allows the implementation of these modes in a three-dimensional circular duct geometry.

Azimuthal and radial pressure distributions of test cases with different mode orders show a good agreement with the results of analytical solutions. The analysis of the mode implementation at different background flows

shows a sufficient accuracy when examining the axial wavelengths. The expected contraction of  $\lambda_{ax}$  can be observed. The investigation of the mode propagation angle  $\phi$ , verifies the capability of the developed boundary condition of implementing spinning modes. A good agreement in pressure distribution and axial wavelength of CAA and analytics can be attained regarding the excitation of superposed modes.

Future developments are aimed at the extension of the boundary condition for both, circular and annular ducts. This aspect makes the boundary condition suitable for geometries with hub, e.g. aircraft engine inlets with spinners and thus allows an acoustic analysis of these geometries.

## 6. ACKNOWLEDGMENTS

The authors would like to thank Jan Delfs, Roland Ewert, Jürgen Dierke, and the whole department AS-TEA of the DLR Braunschweig for their support and the helpful discussions. Furthermore, we would like to thank the DFG (German Research Foundation) for the financial support.

## REFERENCES

1. Smith MJT. Aircraft noise. Cambridge aerospace series. Cambridge and New York: Cambridge University Press; 1989.
2. Kaji S, Okazaki T. Generation of sound by rotor-stator interaction. *Journal of Sound and Vibration*. 1970;13(3):281–307.
3. Morfey CL. Rotating pressure patterns in ducts: Their generation and transmission. *Journal of Sound and Vibration*. 1964;1(1):60–87.
4. Tyler JM, Sofrin TG. Axial Flow Compressor Noise Studies. Warrendale and PA: SAE International; 1962.
5. Ozyoruk Y, Long LN. Computation of sound radiating from engine inlets. *AIAA Journal*. 1996;34(5):894–901.
6. Farassat F, Myers MK. Extension of Kirchhoff's formula to radiation from moving surfaces. *Journal of Sound and Vibration*. 1988;123(3):451–460.
7. Schnell R. Investigation of the Tonal Acoustic Field of a Transonic Fanstage by Time-Domain CFD-Calculations With Arbitrary Blade Counts. In: ASME Turbo Expo 2004: Power for Land, Sea, and Air; June 14–17, 2004. p. 1763–1773.
8. Weckmüller C, Guerin S, Ashcroft G. CFD/CAA Coupling Applied to DLR UHBR-Fan: Comparison to Experimental Data. In: 15th AIAA/CEAS Aeroacoustics Conference (30th AIAA Aeroacoustics Conference); .
9. Schönwald N. Effiziente Simulation der Schallausbreitung in anwendungsnahen Triebwerkskonfigurationen. Berlin: Univ.-Verl. der TU; 2010.
10. Tam CKW, Webb JC. Dispersion-Relation-Preserving Finite Difference Schemes for Computational Acoustics. *Journal of Computational Physics*. 1993;107(2):262–281.
11. Delfs J. Numerical Simulation of Aerodynamic Noise with DLR's aeroacoustic code PIANO: Manual for Version 5.2; 2008.
12. Bogey C, Bailly C. A family of low dispersive and low dissipative explicit schemes for flow and noise computations. *Journal of Computational Physics*. 2004;194(1):194–214.
13. Hu FQ, Hussaini MY, Manthey JL. Low-Dissipation and Low-Dispersion Runge–Kutta Schemes for Computational Acoustics. *Journal of Computational Physics*. 1996;124(1):177–191.
14. Roland Ewert, Oliver Kornow, Jan Delfs, Thomas Roeber, Marco Rose. A CAA Based Approach to Tone Haystacking. In: 15th AIAA/CEAS Aeroacoustics Conference (30th AIAA Aeroacoustics Conference). Aeroacoustics Conferences. American Institute of Aeronautics and Astronautics; 2009. Available from: <http://dx.doi.org/10.2514/6.2009-3217>.